Time-dependent and coating modulation of tomato response upon sulfur nanoparticles internalization and assimilation: An orthogonal mechanistic investigation Yi Wang a,†,*, Chaoyi Deng a,†, Lijuan Zhao b, Christian O. Dimkpa a, Wade H. Elmer c, Bofei Wang ^d, Sudhir Sharma ^e, Zhenyu Wang ^f, Om Parkash Dhankher ^e, Baoshan Xing ^e, Jason C. White ^{a*} ^aDepartment of Analytical Chemistry, The Connecticut Agricultural Experiment Station, 123 Huntington St., New Haven, CT 06511, USA ^bState Key Laboratory of Pollution Control and Resource Reuse, School of Environment, Nanjing University, Nanjing 210023, China ^cDepartment of Plant Pathology and Ecology, The Connecticut Agricultural Experiment Station, 123 Huntington St., New Haven, CT 06511, USA ^dComputational Sciences, The University of Texas at El Paso, 500 West Univ. Ave., El Paso, TX, 79968, USA ^eStockbridge School of Agriculture, University of Massachusetts Amherst, Amherst, MA, 01003, USA ^fInstitute of Environmental Processes and Pollution control, and School of Environment and Civil Engineering, Jiangnan University, Wuxi 214122, China **Author Contributions** Yi Wang[†] and Chaoyi Deng[†] contributed equally. *Corresponding author Yi Wang; e-mail: Yi.Wang@ct.gov; Phone: (203) 974-8449; Fax: (203) 974-8502. Jason C. White; e-mail: Jason. White@ct.gov; Phone: (203) 974-8440; Fax: (203) 974-8502.

Abstract

32

33

34

35

36

37

38

39

40

41

42

43

44

45

46

47

48

Nano-enabled strategies have recently attracted attention as a sustainable platform for agricultural applications. Here, we present a mechanistic understanding of nanobio-interaction through an orthogonal investigation. Pristine (nS) and stearic acid-surface modified (cS) sulfur nanoparticles (NPs) as a multi-functional nanofertilizer were applied to tomato (Solanum lycopersicum L.) through soil. Both nS and cS increased root mass by 73% and 81%, and increased shoot weight by 35% and 50%, respectively, compared to the untreated controls. Bulk sulfur (bS) and ionic sulfate (iS) had no such stimulatory effect. Notably, surface modification of S NPs had a positive impact, as cS yielded 38% and 51% greater shoot weight compared to nS at 100 and 200 mg/L, respectively. Moreover, nS and cS significantly improved leaf photosynthesis by promoting the linear electron flow, quantum yield of photosystem II, and relative chlorophyll content. The time-dependent gene expression related to two S bioassimilation and signaling pathways showed a specific role of NPs surface physicochemical properties. Additionally, a time-dependent Global Test and machine learning strategy applied to understand the NP surface modification domain metabolomic profiling showed that cS increased the contents of IA, tryptophan, tomatidine, and scopoletin in plant leaves, as compared to the other treatments. These findings provide critical mechanistic insights into the use of nanoscale sulfur as a multifunctional soil amendment to enhance plant performance as part of nano-enabled agriculture.

50

51

52

49

Keywords: Nano-enabled agriculture, sulfur nanoparticles, surface coating, gene expression, metabolomics

53

54

Introduction

Although the advancements of the Green Revolution significantly improved global agricultural output, many of those technological advances have proven to be unsustainable, particularly given the rapidly increasing population and changing climate. For example, the application and/or utilization efficiency of most agrichemicals is often below 30%, with some pesticides being below 5%. Consequently, growers may overapply fertilizers and pesticides to ensure satisfactory yields, but this results in significant negative impacts on the environment. Furthermore, as the world's population continues toward 10 billion by 2050, it is clear that agricultural production will need to increase by an approximately 70% to meet the burgeoning food demand. Importantly, conventional agriculture will be unable to meet that challenge and as such, the development and adoption of innovative and sustainable strategies to increase food production are desperately needed.¹²

Sulfur (S) is a critical nutrient for plant growth, being a key component of amino acids and protein synthesis. In addition, several S-containing amino acids are critical to glutathione metabolism.³ However, given the decades-long trend towards cleaner energy sources and decreased use of high S-containing fossil fuels, many agricultural soils have become S deficient.⁴ These deficiencies have resulted in the need for direct application of bulk S to soils as a mitigation measure. However, as noted above, the efficiency of S delivery and subsequent utilization by plants when applied in bulk form is relatively low. Similar to other agrichemicals, this leads to potential over-application of S, which can cause soil acidification, mobilize co-present toxic metals in soil, negatively impact soil structure and fertility, and be generally detrimental to crop health. Consequently, novel approaches to S management are needed.

A growing number of studies have demonstrated the potential of nanoscale nutrients to enhance the growth of a range of crops under non-stressed and stressed conditions.^{5–8} Nutrients at

the nanoscale have greater bioavailability and activity, demonstrating not only enhanced rates of uptake and utilization, but also more intense activation of important secondary metabolite and defense pathways that lead to greater growth and tolerance to biotic/abiotic stress. Although the literature on the use of nanotechnology in agriculture has developed rapidly, a significant focus has been placed on metal or metal oxide NPs. As noted above, S is an important nutrient; however, little is known about the potential benefits of nanoscale S. Although a small number of studies have shown that nanoscale S can suppress plant disease and enhance growth on the biotic stress of disease pressure, 9.10 the potential specific fertilization effects are poorly understood. Stearic acid modification is a common strategy employed to mitigate the tendency of NPs to agglomerate. This modification reduces the surface energy and thereby facilitate the dispersion and stabilization of NPs as surfactants. Additionally, stearic acid finds application as a food or fertilizer additive. However, the application of stearic acid surface modification in agriculture is rare, and there is little mechanistic understanding on the positive impacts of S as a function of particle size, time under exposure, and surface coating.

The objective of the current study is, therefore, to gain a mechanistic understanding of the impacts of nanoscale S on the growth of tomato plants under greenhouse conditions as a function of particle size, chemical modification, and time under exposure. To this end, we investigated the influence of nanoscale surface coating on the biosynthesis of functional metabolites and gene expression during plant growth. An orthogonal and time dependent approach analyzing metabolite and gene expression data using machine learning approaches, including multivariate partial least-squares-discriminant analysis (PLS-DA) and Debiased Sparse Partial Correlation (DSPC) network analyses were used to understand the dynamics and mechanisms associated with S amendment.

This work demonstrates the significant potential of nanoscale S as a multifunctional soil amendment to promote crop performance as part of sustainable nano-enabled agriculture.

Results

Material characterization

Images from SEM-EDS, TEM, and XRD patterns are shown in SI Figure S2-4. Both uncoated and coated nanoscale S showed a uniform spherical morphology with average particle sizes of 65 ± 7.7 and 38 ± 5.9 nm, respectively. The crystal diffraction patterns (SI Figure S2) confirmed an orthorhombic crystal structure (S8) of nS, cS, and bulk S ¹⁵. The zeta potential values of nS, cS, and bS in 100 mg/L suspended in DI at pH 7 were -23.6 \pm 0.4, -33.5 \pm 0.3, and -13.9 \pm 4.3, respectively (SI Figure S5). The EDS analysis confirmed the elemental composition of nS and bS as pure S, and cS as a combination of S and C. The dissolution of all the three S based compounds in DI was less than 0.4% at 15 days (SI Figure S6).

The enhanced plant biomass and photosynthesis

In the first greenhouse study as shown in Figure 1, no changes were observed at day 4 as a function of treatment. At day 8, cS increased root mass by 41.1% compared to the control, and by 27.9% compared to bS. Importantly, at day 16 both shoot and root fresh weight were significantly increased by nS and cS than control but not by bS (p < 0.05). The increase in root weight was 57.5% and 65.1% for nS and cS than control, and 94.3% and 103.6% compared to bS, respectively; the increase in shoot weight was 35.1% and 50.0%, respectively, compared to controls. Similar results were confirmed in the second greenhouse experiment (Figure 1 and SI Figure S9); nS at 100 and 200 mg/L increased shoot mass by 32.1%-38.8% relative to the control; cS increases were 39.6%-57.5%, respectively. In terms of root biomass, the nS and cS groups were 4.0-4.3g and 4.6-5.1g

respectively; while iS showed a reduced root biomass (1.4-1.9g) compared to the untreated control (2.85±0.86g). Surface modification of S nanoparticles had a significant beneficial impact on the plants; cS treated tomato had 13.5% greater shoot weight than nS at 200 mg/L. However, iS at both concentrations decreased shoot biomass 32.6-38.9% compared to the control, whereas bS and iS had no impact on root biomass, regardless of concentration. A similar trend was evident with plant height (SI Text S7). These findings demonstrate the considerable potential of nanoscale S to promote early-stage growth. A number of nanoscale amendments have been shown to increase biomass, although less data is available on nanoscale sulfur amendments, particularly as a function of surface coating.

The effect of S treatment on photosynthesis was studied. Figure 2 shows the relative chlorophyll content, which is an indirect measure of photosynthesis and productivity, as well as an important agronomic indicator for growth. Specifically, nS and cS yielded plants with up to 72.0% and 64.9% greater relative chlorophyll content compared to the ionic control, 47.9% and 68.4% greater compared to the bulk S, and 38.5% and 41.3% greater compared to the untreated control. Figure 2 shows the linear electron flow (LEF) of tomato after 35 days' exposure. LEF represents the amount of energy that is being transferred through the chloroplasts following exposure to light. Notably, the nanoscale S treated groups at both 100 and 200 mg/L exhibited significantly greater values (47.3-55.9% for nS and 75.9-79.4% for cS) than the control (37.5%) and all other treatments (19.6–46.9%), demonstrating enhanced electron flow and carbon fixation (p < 0.05). In addition, nS at 100 mg/L significantly increased the quantum yield of Photosystem II (Phi2) (124.8%) compared to the control. Phi2 is a measure of the percentage of incoming light (excited electrons) that goes into Photosystem II (photosynthetic processes) for conversion to

carbohydrates (Figure 2). Importantly, bS and iS at 200 mg/L deceased Phi2 by 35.5 and 39.2% relative to the control, respectively.

The bioavailability of nutritional elements in S-amended soils at 200 mg/L was investigated by three different methods: extraction by DI, DTPA, or CaCl₂. The results (SI Figure S6) show no significant differences between cS, nS, and bS.¹⁰ In addition, due to the relatively low rate of particle dissolution (~2%, SI Figure S5) from nS and cS, it is unlikely that the enhanced growth was due to sulfate release. The results demonstrate that the nS and cS treatments are a promising multifunctional platform that can enhance photosynthesis by multiple mechanisms. In particular, when compared to all other treatments, the nS groups exhibited a significantly higher Phi2 value; while cS had the most pronounced enhancement on LEF levels, suggesting that the effects of nanomaterials on photosynthesis are specific to the material surface properties. A deeper understanding of mechanisms related to each nano S material were further revealed by the gene expression and time-dependent metabolomics discussed below.

S accumulation in root, stem, and leaf tissues

In the unamended controls, the root S concentration increased over day 4 to 8 from 3,879 to 4,498 mg/kg dry weight and decreased at day 16 to 2,445 mg/kg dry weight (Figure 3). At day 4, only cS exhibited an early effect on root S uptake, causing 19.5-25.5% greater S accumulation than all the other groups. However, this trend was reversed from day 8 to day 16. At day 8, nS increased root S accumulation by 37.7% and 10.4% over controls and cS, respectively. However, at day 16, cS increased the root S by 58.2% and 35.3% over the controls and nS, respectively. This finding highlights the dynamics of sulfur acquisition and translocation over time as a function of particle size. Over time, the control group exhibited a consistent pattern with stem and leaf S trending similarly to the root S concentration. Compared to day 4, the stem S content increased

11.1% at day 8 and decreased 25.9% at day 16. Similar to the roots, at day 4 only cS caused significantly higher S uptake in stems (22.5-24.2%) compared to all the other treatments. At day 8, nS yielded the highest stem S concentration among all S types; values were 69.0%, 48.9, and 31.2% higher than the control, cS, and bS, respectively. At day 16, cS yielded significantly more S in stems than the control, nS, and bS by 58.2%, 35.3%, and 138%, respectively. In addition, cS increased leaf S concentration from day 4 to day 16 compared to each control and nS (although not significantly at day 16 compared to nS). Although bS did result in a comparable increase in S accumulation relative to cS, the biomass data suggests that different efficiencies of utilization and distinct pathways are very likely, since the growth of plants was enhanced by nS and cS, but bS did not exhibit the same beneficial effect.

Previously, Wang et al. (2022) demonstrated particulate nanoscale S uptake by tomato roots, with subsequent translocation to leaves. 10, where use of real-time two-photon microscopy successfully provided a 3-D distribution pattern of the in-situ nanoscale sulfur that was a function of both particle size and surface coating. In leaves, S internalized from the soil exposure distributed primarily around the stomata, indicating transport through xylem via the transpiration stream. The translocation and transformation of nanoscale sulfur may play a crucial role in the observed benefits to plants and continues to be a subject of ongoing research. Under nanoscale sulfur treatment, the dominant pathway for sulfur assimilation was through S0, with direct transformation from inorganic S0 to organic S. 10 This results in significantly higher assimilation efficiency compared to the traditional sulfate route that was utilized for the non-nanoscale treatments. Although the current study lacks visual evidence of the localization of S nanoparticles in the tomato plant, such evidence can be assumed from our previous work involving tomato and under similar treatment conditions.

Regulation S assimilation genes

A schematic diagram of targeted genes in the S bioassimilation pathway is shown in Figure 4. The assimilation of S begins in the plant roots; sulfate (SO₄²-) is the primary form for uptake by S transporters. If sulfate becomes limiting in the soil, plants may increase the expression of sulfate transporters to facilitate nutrient acquisition.¹⁷ The gene *ST2.1* is expressed in root pericycle cells, as well as leaf xylem and phloem parenchyma cells,¹⁸ and mediates the uptake of sulfate from the apoplast within the vascular tissues in roots, promoting translocation to young tissues through shoot phloem transport ¹⁸. In Figure 4, an increase in *ST2.1* expression in the root tissue is evident in the control over 4 to 16 days. Conversely, the S treatments have no impact on the expression of *ST2.1* in tomato roots at day 4 relative to the controls. However, at day 8, cS increased root *ST2.1* expression by 174%, 122%, and 121% compared to nS, control, and bS, respectively. Interestingly, by 16 d, root *ST2.1* expression with nS had increased dramatically; levels were 164%, 169%, and 141% over that of cS, bS, and control, respectively. Thus, cS treatment showed an earlier effect than nS on the up-regulation of *ST2.1* gene.

After root uptake, ATP-sulfurylase catalyzes the activation of SO₄²⁻ as the first step of primary S-assimilation in plants and generates adenosine-5'-phosphosulfate (APS), which is then reduced to sulfide (S²⁻) for incorporation into cysteine as catalyzed by cysteine synthase¹⁹. In addition, ATP-sulfurylase activity is modulated in response to oxidative stress and S deficiency.²⁰ As shown in Figure 5, in the control leaves ATP sulfurylase 1 (*ATPSI*) expression remained constant across all 16 days, suggesting no S deficiency or excessive uptake of SO₄²⁻ into the roots.²⁰ At day 4, only cS upregulated *ATPSI* expression by 112% relative to the controls. This finding aligns with the data on S concentration in tomato leaves at day 4. Although additional study is needed to confirm the form of S, it is clear that cS enhanced S uptake, likely by an upregulation of

ATPS1 gene expression at day 4, and this early metabolic change benefited the longer-term growth of the plants. Notably, compared with nS, cS had a greater effect on ATPS1 gene up-regulation. Although nS also cause greater ATPS1 expression in leaves at day 4, the effect was not of statistical significance.

There is also a secondary SO₄²⁻ assimilation pathway whereby APS is phosphorylated in an APS kinase-mediated reaction catalyzed by adenylyl-sulfate reductase (ASR) to produce 3′-phosphoadenosine 5′-phosphosulfate (PAPS).¹⁹ PAPS is involved in the production of many Scontaining methionine-derived (aliphatic) or tryptophan-derived (indolic) secondary metabolites such as glucosinolates (GSs). GSs protect plants against several biotic stress-factors, such as herbivory and pathogenesis, and are required for robust plant-immunity. In the current study, *ASR* gene expression remained constant in the controls for the duration of the experiment. However, at day 4, nS and cS increased the expression of *ASR* by 5.2 and 8.1-fold. relative to the controls, and by 1.9 and 2.8-fold, compared to bS, respectively (Figure 5).

Rhodanese or sulfurtransferases/thiosulfate transferase (TST) catalyze another important S assimilation pathway in plants, ²¹ converting elemental inorganic-S (S⁰) directly to organic-S from appropriate donors to nucleophilic recipients, including cyanide, thiols, and dithiols. In plant cells, TST is present in the mitochondria, chloroplasts, cytoplasm, and plastids. ^{21,22,23} The soluble types of S⁰ donors include polysulfide (S_n²⁻), thiosulfate (S₂O₃²⁻), and tetrathionate (S₄O₆²⁻). ²⁴²⁵ Additional examples include the outer sulfur of ⁻SO₃S⁻ and thiosulfonate ions (RSO₃S⁻). When comparing this with the sulfate pathway, which creates SO₃²⁻ and S²⁻—both detrimental to plant cells—the S⁰ assimilation pathway exhibits greater efficacy and efficiency. It does so by promoting sulfur uptake and utilization through direct inorganic-organic sulfur transformation, thus providing a more advantageous route for plants. ¹⁰ At 8 d, the expression of *TST* was significantly upregulated

by both nanoscale treatments (Figure 4) by 14- and 8-fold, compared to the controls. Importantly, TST expression was unaffected by bS. These findings clearly indicate different pathways of sulfur accumulation and assimilation as a function of particle size; hence, a nano-specific effect.

Gene expression in S-related biosynthetic pathways

A schematic diagram of cysteine, glutathione (GSH), methionine, and ethylene within the S bioassimilation pathway is shown in Figure 5; genes targeted for analysis are highlighted. Cysteine–GSH biosynthesis

Cysteine synthase (CS) produces cysteine (HOOC-CH-CH₂-SH) from S²⁻, which is the primary product of sulfate assimilation, and is a critical reactant in the rate-limiting step for methionine and glutathione synthesis. Cysteine is used for protein synthesis and is linked to the systemic acquired resistance pathway in a number of plant species.²⁶ This critical metabolite also introduces inorganic sulfide into the organic carbon skeleton of other important biomolecules. In the current work, *CS* expression in unamended controls was relatively constant over the duration of the experiment. Across the different treatments, minimal changes in expression were found on day 4; only nS significantly upregulated *CS* expression by 62% over controls. However, by day 8 and 16, the increase in nS treatments were 94% and 130%, compared to controls, and 105% and 93%, compared to bS, respectively. The greatest increase by cS treatment was evident at day 16, with values being 75% greater than the control, and 47% than the bS. Interestingly, *CS* expression in nS treatment was 161.8% greater than cS at day 8, whereas there were no differences as a function of coating at day 16. Importantly, expression levels with bS were statistically equivalent to the untreated controls, denoting a nanoparticle-specific effect.

GSH controls the redox states of many biomolecules, and also mediates enzymatic activity, detoxification of xenobiotics and reactive oxygen species, and influences plant growth and

development. ^{18,27} Gamma-glutamylcysteine synthetase (γGCS) catalyzes the first rate-limiting step in GSH production, and involves the ATP-dependent condensation of cysteine and glutamate to form the dipeptide gamma-glutamylcysteine. ¹⁸ In the controls, GSHI expression was constant from day 4 to day 16. Conversely, at day 4 nS significantly increased GSHI expression of by 1.4-fold over bS. At 8 d, cS increased GSHI expression over all other treatments. Glutathione-S-transferases (GST) are important phase II detoxification enzymes that catalyze the conjugation of GSH to endogenous and exogenous electrophilic compounds. Several GST enzymes are known to possess glutathione peroxidase activity and participate in antioxidative defense. Interestingly, the expression of GST in the controls was unchanged across the 16-day growth period and was unaffected by S based treatments, indicating no antioxidative stress was induced.

Cysteine-methionine-ethylene biosynthesis

Methionine is an essential amino acid and a fundamental precursor in metabolism through its primary metabolite, S-adenosylmethionine, which modulates the levels of several key biomolecules, including ethylene, polyamines, and biotin. Changes in gene expression of ethylene responsive methionine synthase (*METS*) were similar to that of *CS*. Specifically, *METS* expression in unamended controls was constant on day 4, 8, and 16. However, on day 4 nS significantly upregulated *METS* expression by 65% and 69% over controls and cS, respectively. By day 8, the nS-mediated increase had disappeared, although cS had then activated *METS* expression. This effect was greatest at 16 d, with cS increasing expression by 101%, 81%, and 199% over controls, nS, and bS, respectively. Both cS and bS did not cause any significant changes compared to the controls at day 8 and 16.

In plants, the ethylene pathway is integral to a range of developmental and signaling processes. Ethylene is regarded as a multifunctional phytohormone that regulates both growth and

senescence, promoting or inhibiting these processes as a function of concentration, timing, and plant species. As shown in Figure 4, the first step of ethylene biosynthesis involves S-adenosylmethionine (SAM) synthase catalyzing the reaction of ATP and methionine to form SAM.²⁸ SAM mediates the transmethylation of proteins, nucleic acids, polysaccharides and fatty acids,²⁹ which is vital in epigenetic regulation, RNA metabolism, and post-translational control of protein function in plants.³⁰ Importantly, nS upregulated the expression of S-adenosylmethionine synthase 2 (*SAM2*) by 81-162% over all other treatments at day 8.

1-Aminocyclopropane-1-carboxylic acid (ACC) oxidase (ACOI) catalyzes the final step in ethylene biosynthesis, converting ACC to ethylene in the presence of Fe(II).³¹ An important temporal effect was observed at day 8 in the controls, when the expression ACOI was upregulated 7.0- and 1.3-fold greater than day 4 and day 16, respectively. nS increased ACOI gene expression 2.1-, 2.3-, and 7.4-fold over bS, cS, and controls at day 4; and 5.0- and 2.0- fold over bS and cS at day 8, respectively. At day 16, all S based treatments resulted in 1.5 – 2.5-fold greater ACOI expression than controls.

Ethylene response factors (ERFs) are AP2/ERF superfamily proteins that are highly conserved in the plant kingdom and are involved in responses to environmental stimuli. In controls, the expression of *ERF4* was gradually increased from day 4 to day 16. However, bS resulted in greater *ERF4* expression than nS and cS by 79% and 221% at day 4, and by 74% and 137% at day 8. ERFs influence fruit ripening, induction of flowering, loss of chlorophyll, directed tissue necrosis, stem shortening, abscission of plant tissues, epinasty (stem bending), and dormancy. Ethylene can also be produced when plants are injured, either mechanically or by disease. Excessive ethylene exposure can lead to stunted growth, leaf epinasty (downward curling), premature leaf senescence, and even plant death in extreme cases.^{32,33} Ethylene inhibits vegetative

growth by restricting cell elongation, mainly through cross-talk with auxins, ³⁴ and also inhibits cell division, DNA synthesis, and growth in the meristems of roots, shoots, and axillary buds, without influencing RNA synthesis. ³⁵ The significantly lower *ERF4* expression in nS and cS groups indicates that no stress was induced by these applications as compared to bS.

In summary, *CS* expression was significantly increased in response to nS over time. However, bS treatments showed no impact on *CS* expression, and on day 8, nS treatment exhibited a notably higher expression than cS. cS significantly increasing METS expression on day 8 and 16, and nS briefly upregulating it on day 4. nS upregulated the expression of SAM2 on day 8, outperforming other treatments. Notably, treatment with nS increased ACO1 gene expression compared to bS, cS, and controls at various time points, with the most substantial impact observed on day 8. These results demonstrate the time-dependent nature of the processes and highlight a crucial narrow temporal window around day 8 with regard to the distinct impacts of nS and cS treatments, respectively. In contrast, the expression of ERF4, was notably higher in the bS group, demonstrating that nS and cS do not induce the same level of stress as bS.

Metabolite profile as a function of S

The plant metabolome, the global profile of the composition of metabolites, mirrors transcriptional changes as a function of conditions and provides additional information on the function of the plant immune system since these biomolecules represent the end products of regulatory processes ^{36,37}. Accordingly, metabolomics analysis was performed at different time points to understand the dynamics and mechanisms of nanoscale S benefits to tomato, and to support a comparative analysis with the findings of our transcription results. In total, more than two hundred important plant metabolites were identified and semi-quantified in tomato leaves. The results of enrichment analysis were shown in SI Figure S7 and S8.

The partial least-squares-discriminant analysis (PLS-DA) score plot provides an overview of the clustering between different S treatments (Figure 6). At 8 d, there was a clear separation of nS from all the other treatments along the first and second principal components. Additional PLS-DA plots were constructed with groups at 8 d and 16 d for comparison of temporal effects. At 8 d, nS and control were well separated from each other, and both were separated from bS and cS; interestingly, bS and cS remained close to each other (Figure 6). At 16 d, a different pattern was evident, with nS continuing to show a clear separation from control and bS; however, the difference between cS and bS was now evident at this later time point. This result demonstrates the importance of nano-fertilizer applications at early stages of plant growth, as well as the importance of size and coating of the applied materials with regard to the temporal dynamics of response. A heatmap (Figure 7) shows the metabolites that are important in plant growth and development; a systematic positive modulation of metabolic processes in leaves is clearly evident upon nS and cS treatment, highlighting the overall beneficial impact on plant metabolism.

To investigate underlying mechanisms and to determine which metabolites are closely related to each other and/or directly tied to increased plant growth, a correlation analysis between plant agronomic variables and metabolomic profiles was conducted by calculating the Pearson correlation coefficient (Figure 7 and Figure 8). Based on this analysis, a discussion of important metabolites follows below, including amino acids, indoles, flavonoids/pigments, alkaloids, hormones, methionine-containing metabolites, and some other S-containing metabolites. In the unamended control groups, most of the metabolites increased with the growth of plants. From day 8 to day 16, the content of indoleacrylic acid (IA), tryptophan, pelargonidin, rutin, quercetin,

tomatidine, scopoletin, solasodine, jasmonic acid (JA), erysolin, and Met-Phe-His increased 174%, 181%, 259%, 538%, 698%, 32.9%, 34.8%, 54.7%, 63.2%, 66.6%, and 121.0%, respectively.

Metabolites enhanced by cS and the related effects

353

354

355

356

357

358

359

360

361

362

363

364

365

366

367

368

369

370

371

372

373

374

375

Significant differences in these values as a result of S type were also evident. Among all the treatments, relatively greater accumulation of IA, tryptophan, tomatidine, and scopoletin were found in cS treated plant leaves. At day 8, only cS exhibited a significant increase in IA compared to controls by 28.7%; this value was 39.8% and 37.0% higher than in nS-treated plants at day 8 and day 16, respectively. No increase was observed in plants treated with nS or bS. At day 16, the IA content with cS and nS was 62.6% and 18.7% greater than bS, as well as 107% and 51.1% greater than controls, respectively. At day 8, nS and cS yielded higher tryptophan accumulation compared to controls by 30.5 and 25.3%, respectively. Conversely, bS had no impact on tryptophan production at day 8. At day 16, tomatoes treated with cS had 47.0% more tryptophan in leaves than nS, and 66.5% more than bS. Compared with the control, tryptophan content with cS and nS was 111% and 43.6% greater, respectively. At day 8, tomatoes treated with cS also had 17.0% and 20.4% more tomatidine and scopoletin than the controls, respectively. IA, also known as 3-(3-indolyl)acrylic acid, is a naturally occurring plant auxin, and plays crucial roles in plant growth and development, including cell elongation, root initiation, apical dominance, and tropical responses. IA is a metabolite derived from tryptophan, an amino acid that animals cannot biosynthesize. Interestingly, tryptophan formation was also increased by both forms of nanoscale S. Tryptophan is utilized in the synthesis of proteins and serves as the structural foundation for numerous plant secondary metabolites which have a wide range of functions in plants, including seed germination, root growth and development, senescence, flowering, and fruit ripening, as well as in the response to biotic and abiotic stresses.³⁸ In addition to auxin, tryptophan is a precursor of indoleamines such as melatonin and serotonin, both of which are critical plant growth regulators.³⁹ The addition of tryptophan has been shown to up-regulate the production of downstream metabolites with commercial or biological value, as well as to promote plant growth by enhancing protein synthesis.⁴⁰ Alkaloids show potent antimicrobial activities against various pathogenic microorganisms, provide plants with protection against predators, and can inhibit the growth of other plants via allelopathy. Specific alkaloids, such as tomatidine from tomato, exhibit both antimicrobial and antifungal properties.⁴¹

Metabolites enhanced by nS and the related effects

376

377

378

379

380

381

382

383

384

385

386

387

388

389

390

391

392

393

394

395

396

397

398

The strongest enhancement was demonstrated by nS in the formation of pelargonidin, solasodine, jasmonic acid, erysolin, N-Acetyl-S-geranyl-L-cysteine (AGC), and metabolites containing methionine. At day 8, nS and cS resulted in 109% and 31.1% greater pelargonidin content than the control, respectively, and tomatoes treated with nS had 59.4% and 49.1% more pelargonidin than cS and bS, respectively. At day 16, pelargonidin content with nS was 26.5% greater than controls, but neither cS nor bS had any impact. At day 8, cS and bS resulted in 29.2% and 23.6% greater solasodine content than controls, respectively. At day 16, solasodine in plants treated with cS was 55.2% and 36.8% (p < 0.1) greater than nS and controls, respectively. At day 8, nS resulted in 135%, 65.9%, and 107% greater JA accumulation than cS, bS, and controls, respectively. At day 16, JA in plants treated with nS and cS was 68.2% and 36.7% greater than bS, and 56.5% and 27.2% greater than controls, respectively. In addition, nS resulted in 23.1% more JA generation in leaves than cS. At day 16, nS showed an increase of 355% and cS showed a 59.7% increase relative to bS respectively. Notably, nS-treated plants had a 185% increase in erysolin compared to cS. At day 16, AGC was significantly increased by nS, showing values 3.64-, 1.05-, and 3.56-fold greater than controls, bS, and cS, respectively. At day 16 with nS, the content of Met-Phe-His increased significantly, reaching values that were 7.0-, 1.4-, and 13.0-fold higher than controls, bS, and cS, respectively. At day 16, nS significantly increased the content of His Met Gly 10.1-, 1.4-, and 8.4-fold more than controls, bS, and cS, respectively. At the cellular level, flavonoids serve as a buffer for ROS gradients and enhance plant response to stressful conditions. These biomolecules are associated with important pigments, and are involved in numerous physiological activities, including color development, as well as the taste and smell of fruits, flowers, and vegetables.⁴² Flavonoids, particularly quercetin derivatives, improve the water and nutrient-accumulation ability of terrestrial plants, interacting with soil constituents by acting as reductants and metal chelators, and also supporting symbiotic associations with N-fixing bacteria which metabolize and modify flavonoids.⁴³ Pelargonidin is a type of plant pigment known as an anthocyanidin and produces a characteristic orange color. JA is an endogenous growth-regulating substance, and is an essential hormone in plants.⁴⁴ Interestingly, the exogenous application of JA has been shown to cause a regulatory effect in balancing growth and defense in plants; JA is directly involved in many physiological processes, including stamen growth, senescence, and root elongation, and promotes certain aspects of plant growth. Erysolin is an isothiocyanate analog found in various species of vegetables, has antimicrobial properties, and is marketed as a nutritional supplement. AGC is a modified form of the amino acid cysteine and has been studied for its potential health benefits. Specifically, AGC can protect against oxidative damage in cells and tissues and exerts anti-inflammatory effects by inhibiting the production of pro-inflammatory cytokines.

The effect of exposure time to nS and cS

399

400

401

402

403

404

405

406

407

408

409

410

411

412

413

414

415

416

417

418

419

420

421

Rutin, quercetin, and ALA levels were increased by the application of nS and cS differently based on time. For example, at day 8, nS and cS yielded 103% and 73.0% greater rutin

accumulation than controls, respectively, and tomato treated with nS had 32.2% more rutin than bS. At day 16, rutin content with cS was 39.5% greater than bS. At day 8, nS and cS increased quercetin accumulation by 93.2% and 77.5% over controls, respectively. Plants treated with nS had 25.9% more quercetin than bS, and at day 16, rutin content in plants treated with cS was 41.2% greater than bS. At day 8, cS and bS significantly increased the ALA content by 74.9% and 72.3% over controls, and 45.6% and 43.4% over nS. At day 16, ALA in the nS treatment was 274%, 69.1%, and 79.5% higher than the controls, bS, and cS, respectively.

422

423

424

425

426

427

428

429

430

431

432

433

434

435

436

437

438

439

440

441

442

443

444

In summary, the application of nS and cS had varying effects on the accumulation of rutin, quercetin, and ALA in plants over time, with nS generally showing greater increases in rutin, quercetin, and ALA levels at day 8, while cS had a notable impact on rutin and quercetin content at day 16. α-Lipoic acid (ALA), a dithiol short-chain fatty acid with strong antioxidative properties,⁴⁵ has been widely used in medicine. ALA has the potential to improve plant tolerance to a wide array of abiotic stresses.⁴⁶ Rutin (vitamin P) is a common dietary flavonoid which is widely distributed in vegetables, fruits, and medicinal herbs.⁴⁷ Rutin is believed to exhibit significant pharmacological activity, including anti-oxidation, anti-inflammation, anti-diabetic, anti-adipogenic, and can serve as a neuroprotective. Rutin can also be a part of hormone therapy and is present in many therapeutic medicinal preparations. Quercetin is a plant pigment and is the aglycone moiety of rutin after hydrolysis. Quercetin is also an antioxidant flavonoid that increases plant tolerance against biotic and abiotic stress by maintaining oxidative balance through interactions with glutathione (GSH), related enzymatic activity, and signal transduction pathways ⁴². Quercetin facilitates several plant physiological processes, including seed germination, pollen growth, antioxidant machinery, and photosynthesis, as well as induces proper plant growth and development.⁴² Both rutin and quercetin are excellent sources of pharmaceutical products,⁴⁸ and the content of both were enhanced by nS and cS. This result is consistent with the enhancement of IA content, given that auxin promotes quercetin production. In turn, the content of quercetin modulates auxin gradients as an auxin transport inhibitor,⁴⁹ thereby enhancing the local auxin content and supporting the processes of cellular growth and differentiation.⁴²

Metabolomic Pathway Profiling of S Treatments

The Pathway Analysis model combines results from pathway enrichment and pathway topology analyses to identify the most significant pathways as a function of treatment. This strategy uses the high-quality KEGG metabolic pathways as the foundation and integrates well-established methods such as univariate and over-representation analyses with Global Test, GlobalAncova, and network topology analysis. This approach is better able to identify subtle but consistent changes in biomolecules and pathways as a function of treatment.

To understand the mechanisms by which nS and cS increased tomato seedling growth, two factors are critical: nanoscale size and particle surface properties. The pathway analyses are presented in Figure 8. An interactive visualization system shown in the metabolome view was implemented to facilitate data exploration. The positive effect of nanoscale S was investigated by comparing nS with bS. At day 8, nS activated 14 out of 16 metabolic pathways compared to bS, including starch and sucrose metabolism, alpha-Linolenic acid metabolism, sphingolipid metabolism, vitamin B6 metabolism, alanine, aspartate and glutamate metabolism, pyrimidine metabolism, stilbenoid, diarylheptanoid and gingerol biosynthesis, tryptophan metabolism, tyrosine metabolism, aminoacyl-tRNA biosynthesis, isoquinoline alkaloid biosynthesis, phenylpropanoid biosynthesis, one carbon pool by folate, and anthocyanin biosynthesis.

The importance of nanoscale surface properties was evaluated by comparing nS and cS. More beneficial effects were caused by nS at day 8. For example, only 1 metabolic pathway, the

glycerophospholipid metabolism pathway, was upregulated by cS at day 8. However, nS upregulated 11 pathways, including indole alkaloid biosynthesis, tryptophan metabolism, vitamin B6 metabolism, isoquinoline alkaloid biosynthesis, tyrosine metabolism, starch and sucrose metabolism, phenylalanine metabolism, sphingolipid metabolism, anthocyanin biosynthesis, and pyrimidine metabolism pathway. But by day 16, 4 metabolic pathways were upregulated by cS, and only 3 were upregulated by nS. Specifically, cS upregulated phenylpropanoid biosynthesis, stilbenoid, diarylheptanoid and gingerol biosynthesis, alanine, aspartate and glutamate metabolism, and starch and sucrose metabolism. Conversely, nS upregulated anthocyanin biosynthesis, flavone and flavonol biosynthesis, and alpha-Linolenic acid metabolism. Significant changes were observed when comparing the metabolic profile at day 8 with that at day 16, indicating a dynamic or time-dependent efficacy of cS treatment. At day 8, cS only upregulated 6 of 17 pathways compared to bS; however, by day 16 that ratio became 10 of 14. Specifically, at day 8 cS upregulated alanine, aspartate and glutamate metabolism, one carbon pool by folate, sphingolipid metabolism, and aminoacyl-tRNA biosynthesis. At day 16, the cS upregulated pathways were one carbon pool by folate, phenylpropanoid biosynthesis, tryptophan metabolism, stilbenoid, diarylheptanoid and gingerol biosynthesis, starch and sucrose metabolism, aminoacyl-tRNA biosynthesis, isoquinoline alkaloid biosynthesis, tyrosine metabolism, sphingolipid metabolism, and indole alkaloid biosynthesis. These results highlight the important potential of tuning nanoscale surface chemistry to maximize the performance and efficiency of agro-nanomaterials, allowing for precise control over interactions with plant systems, and opportunities for targeted metabolomic profiling enhancements.

489

490

488

468

469

470

471

472

473

474

475

476

477

478

479

480

481

482

483

484

485

486

487

Conclusions

This work demonstrates the significant positive effect of S NPs, with different surface physicochemical properties, on the growth, metabolism, and development of tomato. Compared to uncoated nS, S NPs with stearic acid coating resulted in greater plant height, activated leaf photosynthesis including greater LEF and relative chlorophyll value, and importantly, greater S uptake and translocation in plants. Different mechanisms corresponding to each S NPs focusing on the effect of surface modification were demonstrated by an orthogonal approach, including time-dependent gene regulation of related pathways, time-dependent metabolomic profiling understood through machine learning, and particle dissolution assays in a range of media. Importantly, compared with the nS, cS treatment showed earlier and greater effect on the upregulation S uptake and assimilation related genes. Relatively greater accumulation of IA, tryptophan, tomatidine, and scopoletin were found in cS treated plant leaves; while nS showed a stronger enhancement effect in the formation of pelargonidin, solasodine, jasmonic acid, erysolin, AGC, and metabolites containing methionine. The results reveal the importance of surface modification, offering a promising approach to optimize agro-nanomaterial utilization and enhancement of plant growth in a tunable manner, and tailorable to specific agricultural conditions and objectives.

507

508

509

510

511

512

506

491

492

493

494

495

496

497

498

499

500

501

502

503

504

505

Methods

Characterization of sulfur-based nanomaterials

Two different types of sulfur nanoparticles (US Research Nanomaterials, Inc., Houston TX), pristine nanoscale S (nS) and nanoscale S coated with stearic acid (cS), as well as a bulk size S (bS, Fisher Scientific, NJ), were characterized as shown in SI Text S1.

To measure sulfate dissolution from the particles, 200 mg/L S material suspensions in distilled-deionized water (DI) were sonicated for 2 minutes on ice at 120 W (FisherbrandTM Model 120 Sonic Dismembrator) and kept in the dark. Supernatants (30 min at 12,000 rpm at 4°C, EppendorfTM Centrifuge 5810R) were collected at 4 h, 1 d, 4 d, 8 d, and 16 d and were acidified with HNO₃ and analyzed for S content as described below using inductively coupled plasma—optical emission spectroscopy (ICP-OES).

S dissolution and soil bioavailable nutritional elements

Dissolution of the three S based materials, as well as changes in the bioavailable content of macro/micro-elements and soil properties, were determined in soil. Soil amended with nS, cS, bulk S, or equivalent ionic S at 200 mg/L were extracted according to a previous study with some modification ¹¹. Three different methods using CaCl2, DTPA, or DI were used to optimize the extraction efficiency for different elements. Detailed procedures were described in SI Text S2 and SI Figure S1.

Plant cultivation and S treatment

Tomato seeds, *Solanum lycopersicum* L. cv Bonnie Best (a common heirloom variety), were purchased from Harris Seed Co., Rochester NY. The characterization of soil is shown in SI Text S3. The details of the plant cultivation are shown in SI Text S4. The overview of the experiment design is shown in Figure 1a. Prior to transplanting, suspensions or solutions of each S-based compound were prepared in DI and sonicated for 2 min using a probe sonicator to provide a stable dispersion. The suspensions or solutions were mixed into the soil to achieve final concentrations of 100 or 200 mg/L soil (33 and 66 mg/pot, respectively, chosen based on the background S in soil and previous literature ⁹) and mixed manually for 20 min to ensure homogeneity. Soil amended with the same volume of DI served as untreated controls. All prepared

soil was then placed for two days at room temperature to approach equilibrium. To assess the effect of surface properties, plant responses to nS and cS were directly compared. To evaluate the nanoscale specific efficacy of these two S materials, commercial bulk sized S was included. To investigate the time-dependent efficacy of S material amendment and the underlying mechanisms driving those effects, seedlings were treated with nS, cS, and commercial bulk sulfur (bS), and were harvested at specific time points after the transplanting.

An additional replicate greenhouse experiment with longer exposure and growth time (35 d after transplanting) was conducted with a similar design to investigate the effect of concentration. An additional ionic S form, sodium sulfate salt (Na₂SO₄), was included to evaluate the nanoscale specific efficacy and the effect of ionic S (iS). Twelve replicates were established per treatment. Photosynthetic parameters (relative chlorophyll content, leaf thickness, and linear electron flow (LEF)) were measured using a portable PhotosynQ meter (PHOTOSYNQ INC., USA) at 30 d after the transplanting. Harvested tissues were processed as described above.

Elemental analysis

To measure S content, as well as levels of macro- (P and K), secondary (Ca and Mg), and micronutrients (B, Cu, Fe, Mn, Mo, and Zn), tissues were analyzed by ICP-OES (iCAP 6500, Thermo Fisher Scientific, Waltham, MA). Briefly, approximately 200 mg of dry plant tissue samples were ground and weighed. Fine powders were digested in 5 mL plasma pure HNO₃ for 45 min on a hot block at 115 °C. Further digestion was achieved by adding 1 mL of H₂O₂ for a 20 min heating at 115 °C. After cooling, the digests were diluted to 50 mL with DI. For quality control and assurance, blank (no plant tissues), pure nanoscale and bulk S powder, spikes, and standard reference materials (NIST-SRF 1570a and 1547, Metuchen, NJ) were prepared and analyzed

following the same procedure. Yttrium (Y) was used as an internal standard, and a continuing calibration verification sample with a known concentration was evaluated every 15 samples.

RNA isolation and RT-qPCR

To evaluate gene expression, plant tissue samples frozen in liquid N₂ were pulverized in a mortar. Total RNA extraction was done using the PureLinkTM Plant RNA Reagent (InvitrogenTM) and was quantified using a NanoDrop spectrophotometer (Thermo Scientific) determined by the 260/280 absorbance ratio. ¹² RT-qPCR gene amplification was conducted according to our previous procedures as shown in SI Text S5. ¹² The information on the corresponding primers of selected genes are shown in SI Table S1. Result was calculated using the 2^{ΔCt} method.

Metabolomic analysis and data processing

Fresh plant tissue samples that had been frozen in liquid N₂ were freeze-dried for 6 h using a lyophilizer. Dry samples were extracted as described previously.¹⁰ After centrifugation, the supernatants were analyzed on a Waters Acquity ultra-high-performance liquid chromatography (UPLC) system with a Waters Acquity UPLC HSS T3 analytical column (100 Å pore size, 1.8 µm particle diameter, 2.1 mm x 150 mm) held at 40°C and coupled to a Waters Synapt G2Si HDMS high resolution mass spectrometer with details shown in SI Text S6. Data were processed and analyzed using Progenesis QI (v 2.4, Nonlinear Dynamics) for peak picking, feature retention time (RT) alignment, feature quantification, and metabolite identification. All raw files were imported using the "High resolution mass spectrometer" settings with profile data and positive polarity. Statistical analysis and pathway analysis of the metabolites was performed using MetaboAnalyst 5.0 For multivariate analysis, log10(x) transformation was performed for the normalization by sum^{13,14}.

Statistical analysis

A Shapiro–Wilk's W Test of homogeneity was performed on all data before further analysis. A one-way ANOVA followed by a Tukey–Kramer multiple comparison test was conducted (SPSS, IBM Corp.) with the S treatments as fixed factors. Experiment two was similarly analyzed with S treatment and dose as fixed factors. A student's t-test was also used to compare the differences between specific treatments. Statistical significance was determined at p < 0.05. Data are expressed as the mean \pm standard error (SE).

Supporting Information

The Supporting Information is available free of charge at https://pubs.acs.org/doi/XXXX.

Characterization of S based nanomaterials; assays for the dissolution of S and the bioavailable essential element contents in the soil; results of soil property characterization; plant cultivation and S based treatments; RNA isolation and RT-qPCR analysis; data processing of metabolomic analysis; plant height enhanced by the S nanomaterials. Results of the pH and conductivity of soil amended with S based treatment; properties of S based material characterized by TEM, SEM/EDX, XRD and DLS analysis; time-dependent dissolution of S released from S based materials; interactive bar-chart of the metabolite enrichment analysis and the Enrichment Ratio; phenotypic images of tomato plants upon exposure to S based materials; list of targeted genes and their corresponding primers (PDF).

Acknowledgments

This work was supported by USDA-NIFA-AFRI 2020-67022-32416. CD was supported by the National Science Foundation under Grant No. CHE-2001611, the NSF Center for Sustainable Nanotechnology ("CSN"). The CSN is part of the Centers for Chemical Innovation Program.

606

Reference

- 607 (1) Bindraban, P. S.; Dimkpa, C. O.; Angle, S.; Rabbinge, R. Unlocking the Multiple Public
 608 Good Services from Balanced Fertilizers. *Food Security 2018 10:2* 2018, *10* (2), 273–285.
 609 https://doi.org/10.1007/S12571-018-0769-4.
- Bindraban, P. S.; Dimkpa, C. O.; White, J. C.; Franklin, F. A.; Melse-Boonstra, A.; Koele,
 N.; Pandey, R.; Rodenburg, J.; Senthilkumar, K.; Demokritou, P.; Schmidt, S.
 Safeguarding Human and Planetary Health Demands a Fertilizer Sector Transformation.
 Plants, People, Planet 2020, 2 (4), 302–309. https://doi.org/10.1002/PPP3.10098.
- 614 (3) Bela, K.; Riyazuddin, R.; Horváth, E.; Hurton, Á.; Gallé, Á.; Takács, Z.; Zsigmond, L.;
 615 Szabados, L.; Tari, I.; Csiszár, J. Comprehensive Analysis of Antioxidant Mechanisms in
 616 Arabidopsis Glutathione Peroxidase-like Mutants under Salt- and Osmotic Stress Reveals
 617 Organ-Specific Significance of the AtGPXL's Activities. Environ Exp Bot 2018, 150, 127–
 618 140. https://doi.org/10.1016/J.ENVEXPBOT.2018.02.016.
- Dimkpa, C.; Adzawla, W.; Pandey, R.; Atakora, W. K.; Kouame, A. K.; Jemo, M.;
 Bindraban, P. S. Fertilizers for Food and Nutrition Security in Sub-Saharan Africa: An
 Overview of Soil Health Implications. *Frontiers in Soil Science* 2023, 3, 1123931.
 https://doi.org/10.3389/FSOIL.2023.1123931.
- Zhao, L.; Bai, T.; Wei, H.; Gardea-Torresdey, J. L.; Keller, A.; White, J. C.
 Nanobiotechnology-Based Strategies for Enhanced Crop Stress Resilience. *Nat Food* 2022, 3 (10), 829–836. https://doi.org/10.1038/s43016-022-00596-7.
- Hofmann, T.; Lowry, G. V.; Ghoshal, S.; Tufenkji, N.; Brambilla, D.; Dutcher, J. R.;
 Gilbertson, L. M.; Giraldo, J. P.; Kinsella, J. M.; Landry, M. P.; Lovell, W.; Naccache, R.;
 Paret, M.; Pedersen, J. A.; Unrine, J. M.; White, J. C.; Wilkinson, K. J. Technology
 Readiness and Overcoming Barriers to Sustainably Implement Nanotechnology-Enabled
 Plant Agriculture. *Nat Food* 2020, *1* (7), 416–425. https://doi.org/10.1038/s43016-020-0110-1.
- Giraldo, J. P.; Wu, H.; Newkirk, G. M.; Kruss, S. Nanobiotechnology Approaches for
 Engineering Smart Plant Sensors. *Nature Nanotechnology 2019 14:6* 2019, *14* (6), 541–
 553. https://doi.org/10.1038/s41565-019-0470-6.
- Deng, P.; Gao, Y.; Mu, L.; Hu, X.; Yu, F.; Jia, Y.; Wang, Z.; Xing, B. Development Potential of Nanoenabled Agriculture Projected Using Machine Learning. *Proc Natl Acad* Sci USA 2023, 120 (25), e2301885120. https://doi.org/10.1073/PNAS.2301885120.
- Cao, X.; Wang, C.; Luo, X.; Yue, L.; White, J. C.; Elmer, W.; Dhankher, O. P.; Wang, Z.;
 Xing, B. Elemental Sulfur Nanoparticles Enhance Disease Resistance in Tomatoes. ACS
 Nano 2021, 15 (7), 11817–11827. https://doi.org/10.1021/ACSNANO.1C02917.

- Wang, Y.; Deng, C.; Elmer, W. H.; Dimkpa, C. O.; Sharma, S.; Navarro, G.; Wang, Z.;
 Lareau, J.; Steven, B. T.; Wang, Z.; Zhao, L.; Li, C.; Dhankher, O. P.; Gardea-Torresdey, J.
 L.; Xing, B.; White, J. C. Therapeutic Delivery of Nanoscale Sulfur to Suppress Disease
 in Tomatoes: In Vitro Imaging and Orthogonal Mechanistic Investigation. ACS Nano
- **2022**, 16 (7), 11204–11217. https://doi.org/10.1021/ACSNANO.2C04073.
- Gao, X.; Spielman-Sun, E.; Rodrigues, S. M.; Casman, E. A.; Lowry, G. V. Time and
 Nanoparticle Concentration Affect the Extractability of Cu from CuO NP-Amended Soil.
 Environ Sci Technol 2017, 51 (4), 2226–2234. https://doi.org/10.1021/ACS.EST.6B04705.
- (12) Cota-Ruiz, K.; Ye, Y.; Valdes, C.; Deng, C.; Wang, Y.; Hernández-Viezcas, J. A.; Duarte Gardea, M.; Gardea-Torresdey, J. L. Copper Nanowires as Nanofertilizers for Alfalfa
 Plants: Understanding Nano-Bio Systems Interactions from Microbial Genomics, Plant
 Molecular Responses and Spectroscopic Studies. *Science of The Total Environment* 2020,
 742, 140572. https://doi.org/10.1016/J.SCITOTENV.2020.140572.
- Xia, J.; Wishart, D. S. Web-Based Inference of Biological Patterns, Functions and
 Pathways from Metabolomic Data Using MetaboAnalyst. *Nat Protoc* 2011, 6 (6), 743–760. https://doi.org/10.1038/nprot.2011.319.
- 657 (14) Pang, Z.; Chong, J.; Zhou, G.; De Lima Morais, D. A.; Chang, L.; Barrette, M.; Gauthier, C.; Jacques, P. É.; Li, S.; Xia, J. MetaboAnalyst 5.0: Narrowing the Gap between Raw Spectra and Functional Insights. *Nucleic Acids Res* **2021**, *49* (W1), W388–W396. https://doi.org/10.1093/NAR/GKAB382.
- Villevieille, C.; Novák, P. A Metastable β-Sulfur Phase Stabilized at Room Temperature
 during Cycling of High Efficiency Carbon Fibre–Sulfur Composites for Li–S Batteries. *J Mater Chem A Mater* 2013, *I* (42), 13089–13092. https://doi.org/10.1039/C3TA13072J.
- (16) Seleiman, M. F.; Almutairi, K. F.; Alotaibi, M.; Shami, A.; Alhammad, B. A.; Battaglia, M.
 L. Nano-Fertilization as an Emerging Fertilization Technique: Why Can Modern
 Agriculture Benefit from Its Use? *Plants* 2020, 10 (1), 2.
 https://doi.org/10.3390/PLANTS10010002.
- 668 (17) Buchner, P.; Takahashi, H.; Hawkesford, M. J. Plant Sulphate Transporters: Co-Ordination 669 of Uptake, Intracellular and Long-Distance Transport. *J Exp Bot* **2004**, *55* (404), 1765– 670 1773. https://doi.org/10.1093/jxb/erh206.
- (18) Maruyama-Nakashita, A.; Ohkama-Ohtsu, N. Sulfur Assimilation and Glutathione
 Metabolism in Plants. In *Glutathione in Plant Growth, Development, and Stress Tolerance*; Springer, Cham, 2017; pp 287–308. https://doi.org/10.1007/978-3-319-66682 2 13.
- Anjum, N. A.; Gill, R.; Kaushik, M.; Hasanuzzaman, M.; Pereira, E.; Ahmad, I.; Tuteja,
 N.; Gill, S. S. ATP-Sulfurylase, Sulfur-Compounds, and Plant Stress Tolerance. Front
 Plant Sci 2015, 0 (APR), 210. https://doi.org/10.3389/FPLS.2015.00210.

- 678 (20) Prioretti, L.; Gontero, B.; Hell, R.; Giordano, M. Diversity and Regulation of ATP Sulfurylase in Photosynthetic Organisms. *Front Plant Sci* **2014**, *5*, 116466. https://doi.org/10.3389/FPLS.2014.00597.
- Papenbrock, J.; Guretzki, S.; Henne, M. Latest News about the Sulfurtransferase Protein
 Family of Higher Plants. *Amino Acids 2010 41:1* 2010, *41* (1), 43–57.
 https://doi.org/10.1007/S00726-010-0478-6.
- Niu, J. S.; Yu, L.; Ma, Z. Q.; Chen, P. Du; Liu, D. J. Molecular Cloning, Characterization and Mapping of a Rhodanese like Gene in Wheat. *Yi Chuan Xue Bao* **2002**, *29* (3), 266–272.
- Walz, C.; Giavalisco, P.; Schad, M.; Juenger, M.; Klose, J.; Kehr, J. Proteomics of
 Curcurbit Phloem Exudate Reveals a Network of Defence Proteins. *Phytochemistry* 2004,
 65 (12), 1795–1804. https://doi.org/10.1016/J.PHYTOCHEM.2004.04.006.
- 690 (24) Aussignargues, C.; Giuliani, M.-C.; Infossi, P.; Lojou, E.; Guiral, M.; Giudici-Orticoni,
 691 M.-T.; Ilbert, M. Rhodanese Functions as Sulfur Supplier for Key Enzymes in Sulfur
 692 Energy Metabolism. *J Biol Chem* 2012, 287 (24), 19936.
 693 https://doi.org/10.1074/JBC.M111.324863.
- Mora, M.; López, L. R.; Lafuente, J.; Pérez, J.; Kleerebezem, R.; van Loosdrecht, M. C.
 M.; Gamisans, X.; Gabriel, D. Respirometric Characterization of Aerobic Sulfide,
 Thiosulfate and Elemental Sulfur Oxidation by S-Oxidizing Biomass. *Water Res* 2016, 89,
 282–292. https://doi.org/10.1016/J.WATRES.2015.11.061.
- Álvarez, C.; Ángeles Bermúdez, M.; Romero, L. C.; Gotor, C.; García, I. Cysteine
 Homeostasis Plays an Essential Role in Plant Immunity. New Phytologist 2012, 193 (1),
 165–177. https://doi.org/10.1111/J.1469-8137.2011.03889.X.
- (27) Hibi, T.; Nii, H.; Nakatsu, T.; Kimura, A.; Kato, H.; Hiratake, J.; Oda, J. Crystal Structure of γ-Glutamylcysteine Synthetase: Insights into the Mechanism of Catalysis by a Key
 Enzyme for Glutathione Homeostasis. *Proceedings of the National Academy of Sciences* 2004, 101 (42), 15052–15057. https://doi.org/10.1073/PNAS.0403277101.
- (28) Li, S.; Chen, K.; Grierson, D. A Critical Evaluation of the Role of Ethylene and MADS
 Transcription Factors in the Network Controlling Fleshy Fruit Ripening. New Phytologist
 2019, 221 (4), 1724–1741. https://doi.org/10.1111/NPH.15545.
- 708 (29) Roje, S. S-Adenosyl-l-Methionine: Beyond the Universal Methyl Group Donor.
 709 *Phytochemistry* 2006, *67* (15), 1686–1698.
 710 https://doi.org/10.1016/J.PHYTOCHEM.2006.04.019.
- 711 (30) Rahikainen, M.; Alegre, S.; Trotta, A.; Pascual, J.; Kangasjärvi, S. Trans-Methylation 712 Reactions in Plants: Focus on the Activated Methyl Cycle. *Physiol Plant* **2018**, *162* (2), 713 162–176. https://doi.org/10.1111/PPL.12619.

- 714 (31) Dimkpa, C. O.; Merten, D.; Svatoš, A.; Büchel, G.; Kothe, E. Siderophores Mediate
- Reduced and Increased Uptake of Cadmium by Streptomyces Tendae F4 and Sunflower
- 716 (Helianthus Annuus), Respectively. *J Appl Microbiol* **2009**, *107* (5), 1687–1696.
- 717 https://doi.org/10.1111/J.1365-2672.2009.04355.X.
- 718 (32) Iqbal, N.; Khan, N. A.; Ferrante, A.; Trivellini, A.; Francini, A.; Khan, M. I. R. Ethylene 719 Role in Plant Growth, Development and Senescence: Interaction with Other 720 Phytohormones. *Front Plant Sci* **2017**, *8*, 475. https://doi.org/10.3389/FPLS.2017.00475.
- 721 (33) Wawrzynska, A.; Moniuszko, G.; Sirko, A. Links between Ethylene and Sulfur Nutrition
 722 A Regulatory Interplay or Just Metabolite Association? Front Plant Sci 2015, 6 (DEC),
 723 170615. https://doi.org/10.3389/FPLS.2015.01053.
- Vaseva, I. I.; Qudeimat, E.; Potuschak, T.; Du, Y.; Genschik, P.; Vandenbussche, F.; Van
 Der Straeten, D. The Plant Hormone Ethylene Restricts Arabidopsis Growth via the
 Epidermis. *Proc Natl Acad Sci U S A* 2018, *115* (17), E4130–E4139.
 https://doi.org/10.1073/PNAS.1717649115.
- 728 (35) Burg, S. P. Ethylene in Plant Growth. *Proceedings of the National Academy of Sciences* **1973**, 70 (2), 591–597. https://doi.org/10.1073/PNAS.70.2.591.
- 730 (36) Feussner, I.; Polle, A. What the Transcriptome Does Not Tell Proteomics and
 731 Metabolomics Are Closer to the Plants' Patho-Phenotype. *Curr Opin Plant Biol* **2015**, *26*,
 732 26–31. https://doi.org/10.1016/J.PBI.2015.05.023.
- 733 (37) Weckwerth, W. Integration of Metabolomics and Proteomics in Molecular Plant
 734 Physiology Coping with the Complexity by Data-Dimensionality Reduction. *Physiol Plant* 2008, *132* (2), 176–189. https://doi.org/10.1111/J.1399-3054.2007.01011.X.
- 736 (38) Mano, Y.; Nemoto, K. The Pathway of Auxin Biosynthesis in Plants. *J Exp Bot* **2012**, *63* (8), 2853–2872. https://doi.org/10.1093/JXB/ERS091.
- 738 (39) Woodward, A. W.; Bartel, B. Auxin: Regulation, Action, and Interaction. *Ann Bot* **2005**, *95* (5), 707–735. https://doi.org/10.1093/AOB/MCI083.
- 740 (40) Dubouzet, J. G.; Matsuda, F.; Ishihara, A.; Miyagawa, H.; Wakasa, K. Production of
 741 Indole Alkaloids by Metabolic Engineering of the Tryptophan Pathway in Rice. *Plant* 742 *Biotechnol J* 2013, *11* (9), 1103–1111. https://doi.org/10.1111/PBI.12105.
- 743 (41) Bhambhani, S.; Kondhare, K. R.; Giri, A. P. Diversity in Chemical Structures and 744 Biological Properties of Plant Alkaloids. *Molecules 2021, Vol. 26, Page 3374* **2021**, *26* 745 (11), 3374. https://doi.org/10.3390/MOLECULES26113374.
- 746 (42) Singh, P.; Arif, Y.; Bajguz, A.; Hayat, S. The Role of Quercetin in Plants. *Plant Physiology* 747 *and Biochemistry* **2021**, *166*, 10–19. https://doi.org/10.1016/J.PLAPHY.2021.05.023.
- Hassan, S.; Mathesius, U. The Role of Flavonoids in Root–Rhizosphere Signalling:
 Opportunities and Challenges for Improving Plant–Microbe Interactions. *J Exp Bot* 2012,
 63 (9), 3429–3444. https://doi.org/10.1093/JXB/ERR430.

- (44) Katsir, L.; Chung, H. S.; Koo, A. J.; Howe, G. A. Jasmonate Signaling: A Conserved
 Mechanism of Hormone Sensing. *Curr Opin Plant Biol* **2008**, *11* (4), 428–435.
 https://doi.org/10.1016/J.PBI.2008.05.004.
- 754 (45) Lodge, J. K.; Packer, L. Natural Sources of Lipoic Acid in Plant and Animal Tissues.
 755 Antioxidant Food Supplements in Human Health 1999, 121–134.
 756 https://doi.org/10.1016/B978-012543590-1/50010-X.
- 757 (46) Ramadan, K. M. A.; Alharbi, M. M.; Alenzi, A. M.; El-Beltagi, H. S.; Darwish, D. B. E.;
 758 Aldaej, M. I.; Shalaby, T. A.; Mansour, A. T.; El-Gabry, Y. A. E. G.; Ibrahim, M. F. M.
 759 Alpha Lipoic Acid as a Protective Mediator for Regulating the Defensive Responses of
 760 Wheat Plants against Sodic Alkaline Stress: Physiological, Biochemical and Molecular
 761 Aspects. *Plants* **2022**, *11* (6), 787. https://doi.org/10.3390/PLANTS11060787.
- 762 (47) Chua, L. S. A Review on Plant-Based Rutin Extraction Methods and Its Pharmacological
 763 Activities. *J Ethnopharmacol* 2013, 150 (3), 805–817.
 764 https://doi.org/10.1016/J.JEP.2013.10.036.
- 765 (48) Dabeek, W. M.; Marra, M. V. Dietary Quercetin and Kaempferol: Bioavailability and
 766 Potential Cardiovascular-Related Bioactivity in Humans. *Nutrients* 2019, *11* (10), 2288.
 767 https://doi.org/10.3390/NU11102288.
- Ng, J. L. P.; Hassan, S.; Truong, T. T.; Hocart, C. H.; Laffont, C.; Frugier, F.; Mathesiusa,
 U. Flavonoids and Auxin Transport Inhibitors Rescue Symbiotic Nodulation in the
 Medicago Truncatula Cytokinin Perception Mutant Cre1. Plant Cell 2015, 27 (8), 2210–
 2226. https://doi.org/10.1105/TPC.15.00231.

772

774 Figures

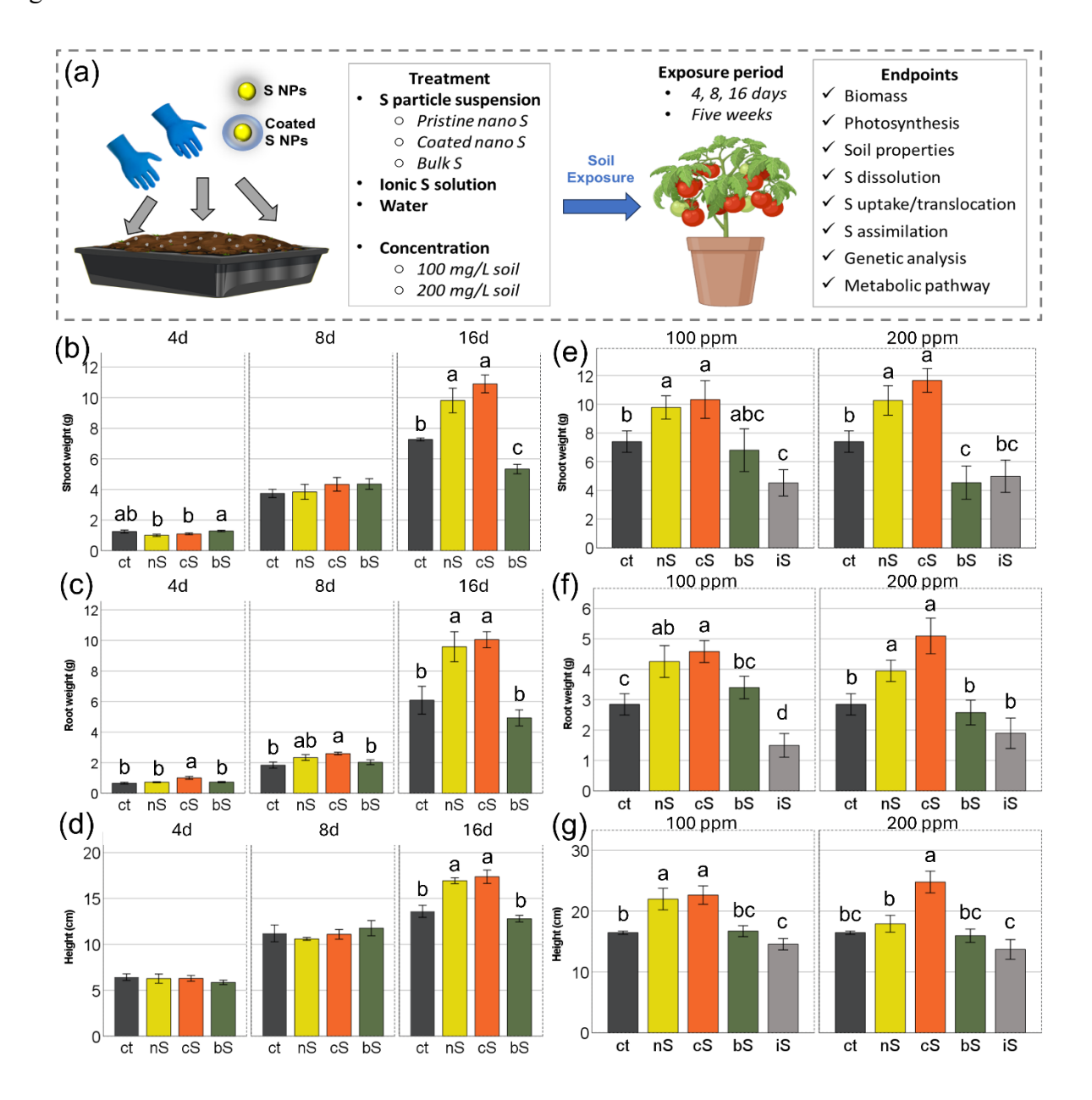


Figure 1. Plant physiological responses of tomato upon S exposure. Figures represent (a) schematic diagram for the overview of the experimental design, (b) shoot weight and (c) root weight, and (d) plant height of tomato upon exposure to nano S (nS), coated nano S (cS), and bulk S (bS) at 200 mg/L soil in first greenhouse study with plants harvested at 4, 8, and 16 days after transplanting; (e) shoot weight and (f) root weight, and (g) plant height of tomato upon

exposure to nS, cS, bS, and ionic S (iS) at 100 and 200 mg/L soil for 35 days in the second greenhouse experiment. In each panel, the black bars represent the controls; yellow and orange bars represent the treatments with uncoated and stearic acid coated S NPs, respectively; dark green and grey bars represent bulk S and ionic S, respectively. Error bars correspond to the s.e.m. Values with different letters within the group of the same time point or concentration are significantly different at p < 0.05.

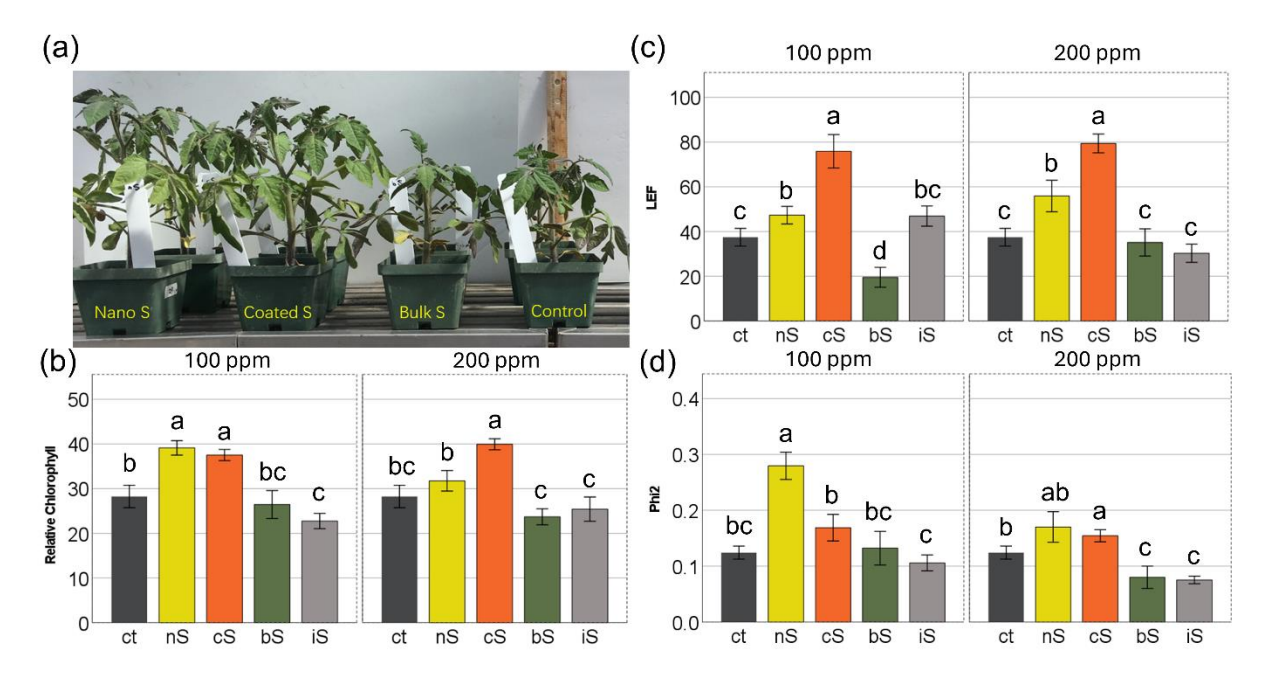


Figure 2. Photosynthetic parameters of tomato leaf upon exposure to nano S (nS), coated nano S (cS), bulk S (bS), and ionic S (iS) at 200 mg/L soil for 35d in the second greenhouse experiment. Figures represent (a) plant image, (b) relative chlorophyll, (c) linear electron flow (LEF), and (d) Phi2 of tomato leaf. In each panel, the black bars represent the controls; yellow and orange bars represent treatments with nS and cS, respectively; dark green and grey bars represent bS and iS, respectively. Error bars correspond to the s.e.m. (n=10). Values with different letters within the group of the same concentration are significantly different at p < 0.05.

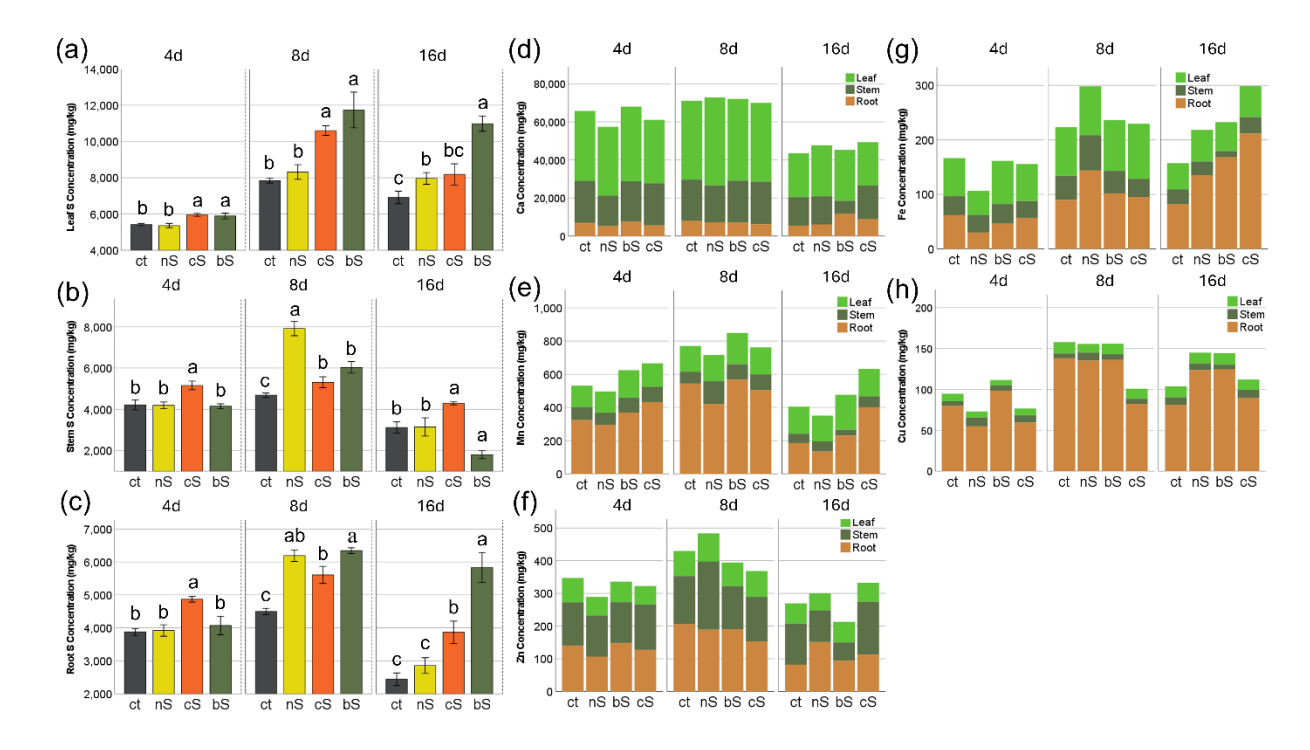


Figure 3. The S content and nutritional element accumulation in tomato plants upon exposure to nano S (nS), coated nano S (cS), and bulk S (bS) at 200 mg/L soil in the first greenhouse study with plants harvested at 4, 8, and 16 days after transplanting. Figures represent S concentration in tomato (a) leaf, (b) stem, and (c) root; And the uptake and distribution of (d) Ca, (e) Mn, (f) Zn, (g) Fe, and (h) Cu content in tomato leaf, stem, and root. Error bars correspond to the s.e.m. (n=5). Values with different letters within the group of the same time point are significantly different at p < 0.05.

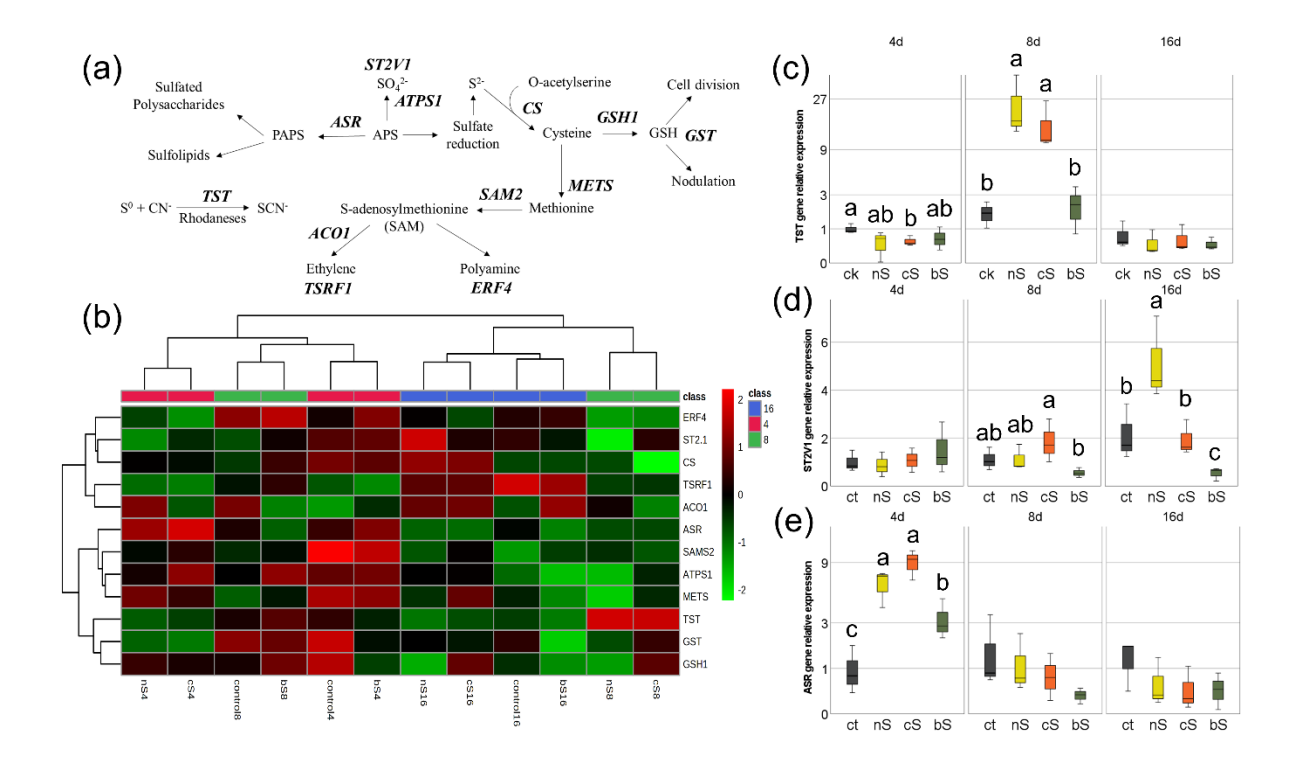


Figure 4. Schematic diagram of the targeted genes in selected pathways of tomato S bioassimilation; relative gene expression, and hierarchical clustering heatmap. (a) Schematic diagram of targeted genes that are related to the S bio-assimilation in tomato plants. (b) Heatmap with hierarchical clustering analysis of the expression of each gene in tomato leaves upon exposure to nano S (nS), coated nano S (cS), and bulk S (bS) at 200 mg/L soil in the greenhouse study with plants harvested at 8, and 16 days after transplanting. Relative expression of S uptakerelated genes includes (c) TST, (d) ST2vI, and (e) ASR in tomato upon soil exposure to nS, cS, and bS at 200 mg/L at 4, 8, and 16 days after transplanting. Values with different letters within the group of the same time point are significantly different at p < 0.05.

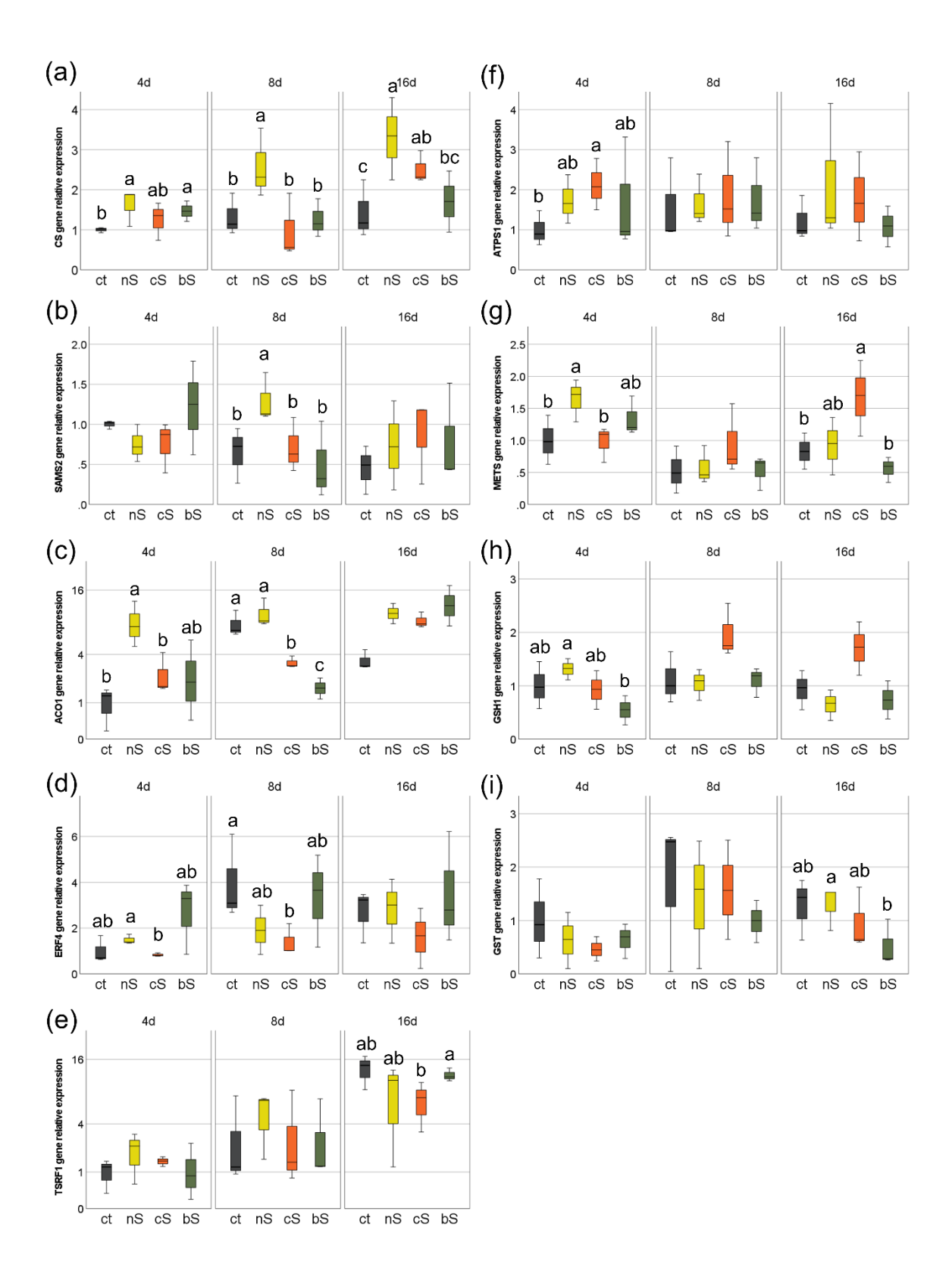


Figure 5. Relative expression of S bio-assimilation-related genes in tomato leaves (CS, SAMS2, ACO1, ERF4, TSRF1, ATPS1, METS, GSH1, and GST). Genes reported include (a) CS, (b) SAMS2, (c) ACO1, (d) ERF4, (e) TSRF1, (f) ATPS1, (g) METS, (h) GSH1, and (i) GST in tomato leaves upon soil exposure to nano S (nS), coated nano S (cS), and bulk S (bS) at 200 mg/L at 4, 8, and 16 days after transplanting. The gene-fold changes were expressed relative to the healthy control plants at day 4. In each panel, the black bars represent the controls; yellow and orange bars represent the treatments with nS and cS, respectively; dark green and grey bars represent bS and iS, respectively. Error bars correspond to the s.e.m. (n=6). Values with different letters within the group of the same time point are significantly different at p < 0.05.

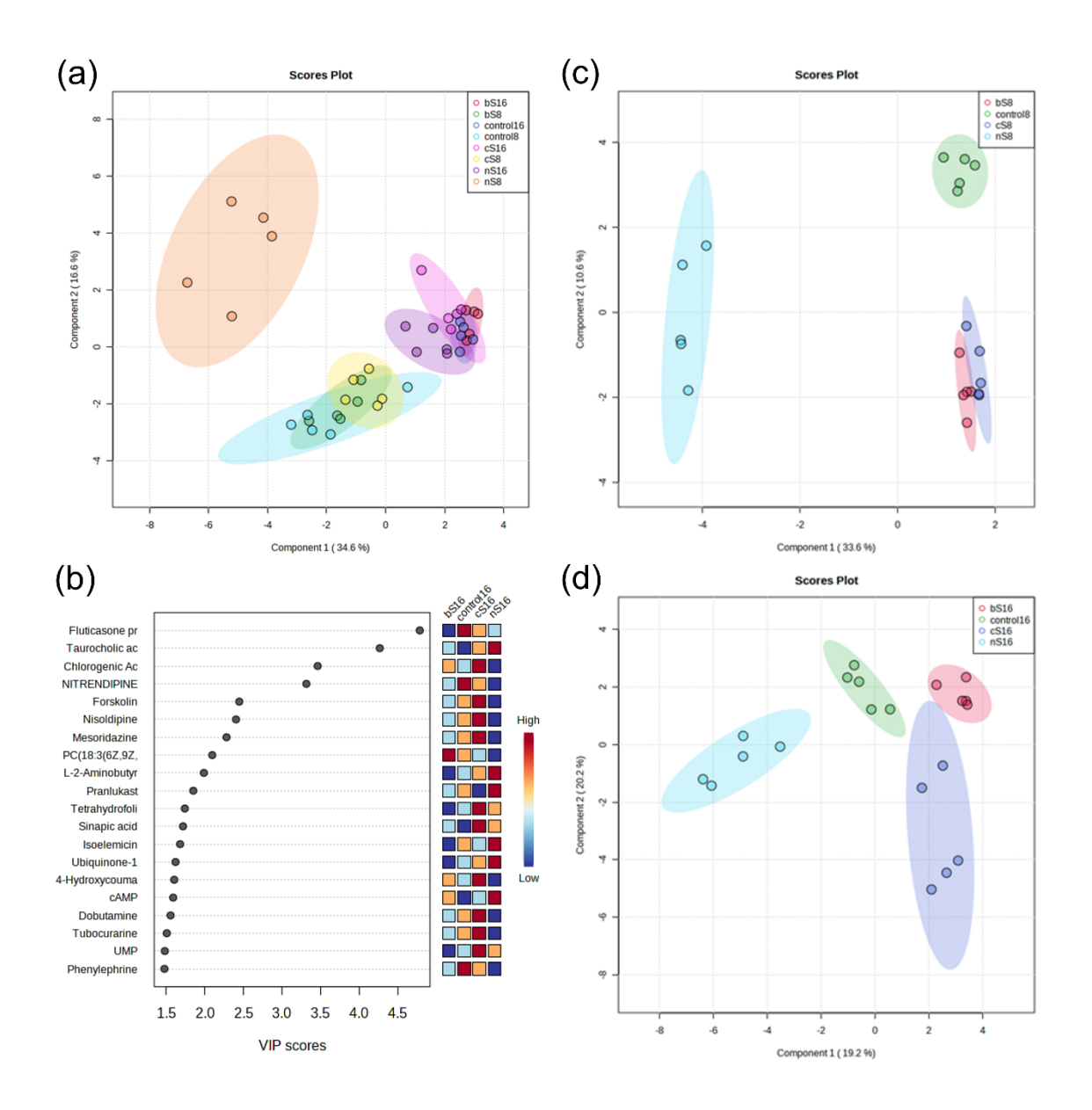


Figure 6. Multivariate analysis of metabolomics data obtained by LC-MS/MS in tomato leaves upon exposure to nano S (nS), coated nano S (cS), and bulk S (bS) at 200 mg/L soil in first greenhouse study harvested at 8, and 16 days after transplanting. (a) Partial least-squares discriminate analysis (PLS-DA) score plots of metabolic profiles in tomato leaves; (b) VIP score plot showing the metabolome pattern at 16 d; PLS-DA score plots of tomato leaves metabolic profiles harvested at different time points as (c) 8 d and (d) 16 d after transplanting.

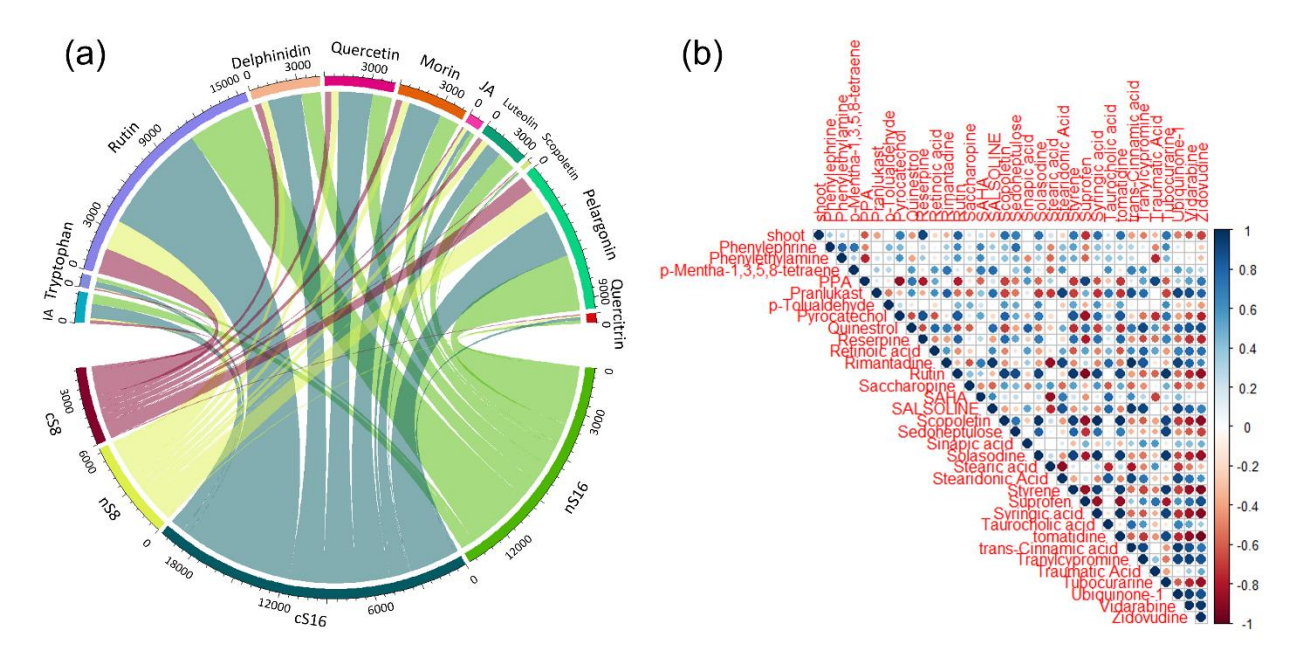


Figure 7. Hierarchical clustering correlation heatmap and chord diagram. (a) Hierarchical clustering correlation heatmap of representative metabolites in tomato leaves upon exposure to nano S (nS), coated nano S (cS), and bulk S (bS) at 200 mg/L soil in first greenhouse study with plants harvested at 4, 8, and 16 days after transplanting; (b) Chord diagram of metabolites improved by nS and cS at 200 mg/L soil in tomato leaves at day 8 and day 16 after transplanting.

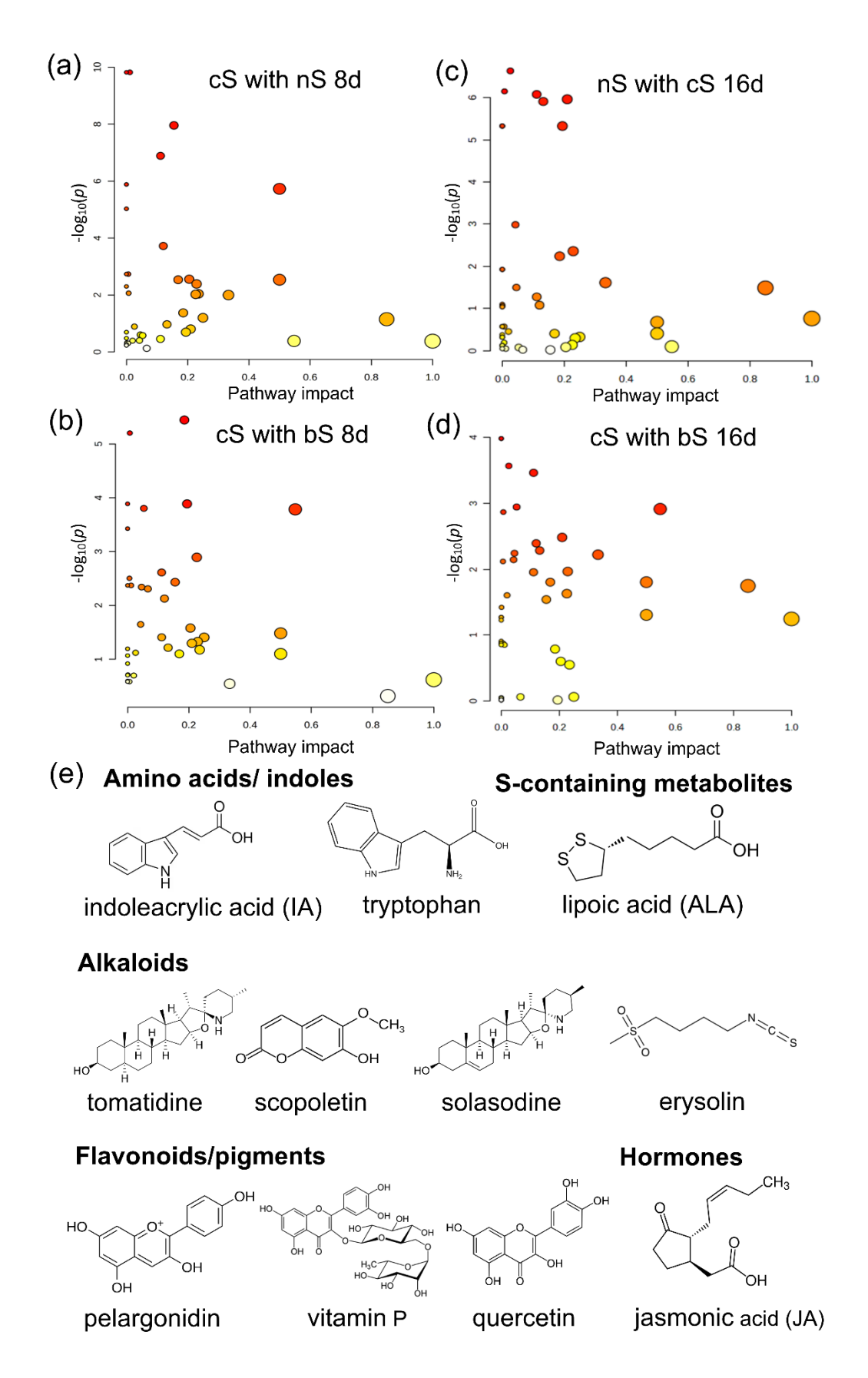
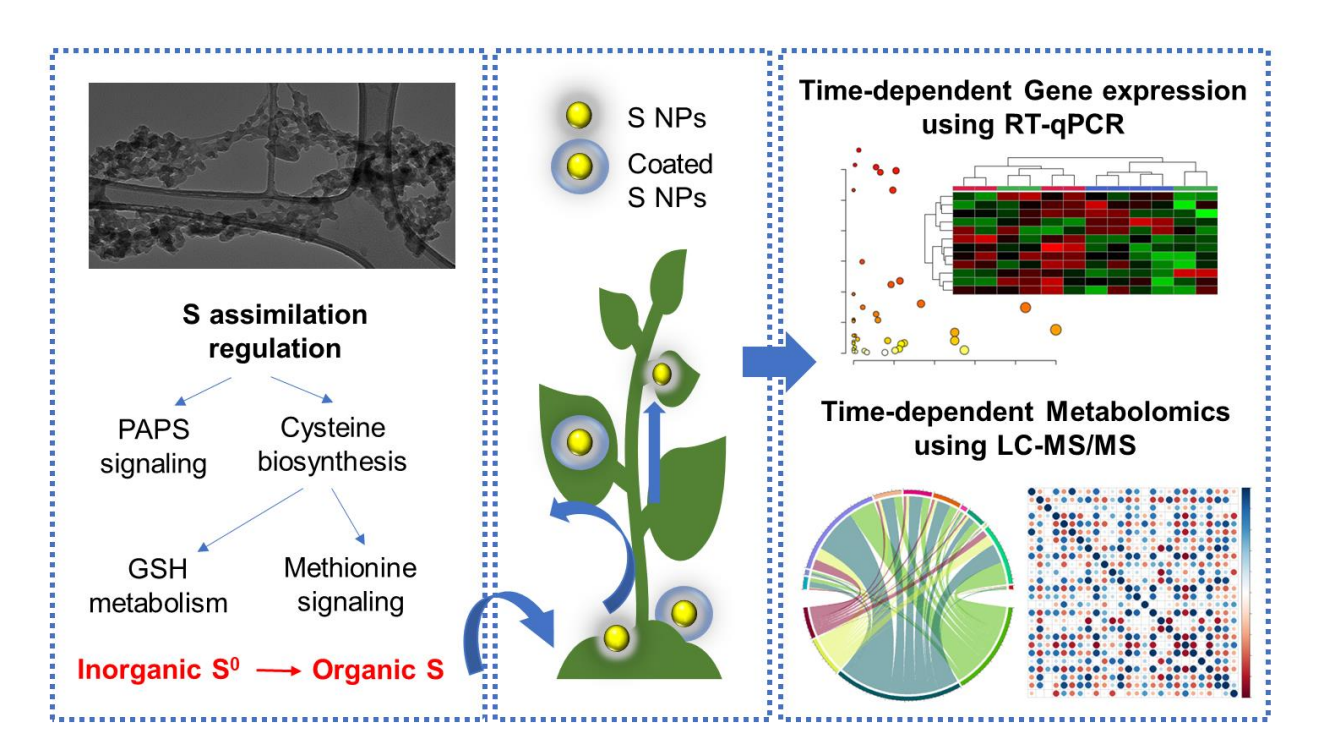


Figure 8. Schematic diagram of proposed metabolic pathways in tomato leaves with the altered metabolite abundance upon exposure to nano S (nS), coated nano S (cS) and bulk S (bS) at 200 mg/L soil in first greenhouse study. Figure represents nS vs. cS with plants harvested at (a) day 8 and (b) day 16 after transplanting; and cS vs. bS with plants harvested at (c) 8 day and (d) 16 day after transplanting. The node color is based on its p-value and changes from red to yellow with the increase of the p-value. The node size reflects the pathway impact values, with bigger nodes corresponding to high impact values. (e) Classification and chemical structures of representative metabolites improved by nS and cS.

For Table of Contents Only

862



863 Graphical Abstract